Nanostructured and recyclable palladium catalysts for hydrogenation of nitroarenes

Xiaopeng Min, Yin Wang*

Department of Civil and Environmental Engineering, University of Wisconsin – Milwaukee, Milwaukee, WI 53201, United States

*Corresponding author:

Yin Wang, 3200 N. Cramer St., Milwaukee, WI 53211, wang292@uwm.edu, 414-251-6446

2024

Abstract

This work reported the preparation of nanostructured palladium (Pd)-based catalysts that consisted of a magnetic core covered by a layer of functionalized mesoporous silica with Pd nanoparticles grown *in situ* within the porous channels (Fe_3O_4@mSiO_2-Pd). The optimum Fe_3O_4@mSiO_2-Pd with fine size and uniformly dispersed Pd nanoparticles was obtained on the amino (-NH_2) functionalized magnetic mesoporous silica support with Na_2PdCl_4 as the Pd source. The performance of the synthesized Fe_3O_4@mSiO_2-Pd was evaluated in the catalytic reduction of nitroarenes in aqueous solution with $H_{2(g)}$ as a reducing agent under ambient pressure and temperature. Compared with commercial Pd/SiO_2, Fe_3O_4@mSiO_2-Pd exhibited significantly improved reactivity in the reduction of various nitroarenes, which were completely reduced to the corresponding aminoarenes. The enhanced performance of Fe_3O_4@mSiO_2-Pd may be attributed to the formation of small and well dispersed Pd nanoparticles within the confined support and the enhanced accessibility of reactive Pd sites within the mesoporous structure. Furthermore, the Fe_3O_4@mSiO_2-Pd catalyst also showed excellent reusability and could be easily collected by an external magnetic field. Results suggested that the synthesized Fe_3O_4@mSiO_2-Pd can be an effective and sustainable catalyst for hydrogenation of nitro-containing compounds.

Keywords: Palladium, mesoporous silica, nanoparticle, nanostructure, catalytic reduction, nitroarene

1. Introduction

Nitroarenes (e.g., nitrobenzene, nitrophenol, nitrotoluene, nitrobenzoic acid, etc.) are a class of structurally related chemicals increasingly detected in various water sources [1]. Their presence can pose negative effects on human health even at very low concentration, and cause long-term adverse influences on aquatic ecosystems [2]. For example, nitrobenzene is a widely used industrial chemical and a proven human carcinogen [3]. Great efforts have been devoted to investigating the removal of nitroarenes. Due to the electron-withdrawing nature of the nitro group on the benzene ring, direct oxidation process (e.g., Fenton process, heterogeneous catalytic ozonation, and UV/H_2O_2 photodegradation) can be ineffective and/or require high energy consumption [4, 5]. Nitroarenes could be transformed to aromatic amines and mineralized by specific bacteria under anaerobic condition during biological treatments [6]. However, the anaerobic process is usually slow and requires excess electron donor substrate [7]. Meanwhile, catalytic hydrogenation has been reported as a beneficial method for nitroarene destruction because of the fast kinetics and clear reaction routes. Moreover, the reaction products (e.g., aromatic amines) of nitroarene reduction may be used as organic intermediates in the preparation of value-added chemicals such as dyes, polymers, pharmaceuticals, agrochemicals, and natural products [8].

Because of the high activity, stability, and selectivity, palladium (Pd)-based hydrogenation catalysis has emerged as a promising water purification strategy for reductive destruction of waterborne contaminants, including halogenated compounds (e.g., chlorophenol, fluoroarenes),

oxyanions (e.g., nitrate, nitrite, bromate, chlorate, and perchlorate), and N-nitrosamines (e.g. N-nitrosodimethylamine) [9-17]. In catalyzing nitroarene reduction, Pd nanoparticles (NPs) have been proven to be highly active for the hydrogenation of nitrophenol to aminophenol and the activity was size-dependent [18]. However, bare Pd NPs tend to aggregate in water to form large bulk precipitates due to the van der Waals forces and high surface energy, which could compromise the catalytic activity and stability of the NPs [19, 20]. Furthermore, direct use of small-size NPs may induce unintended secondary pollution to the treated water, leading to increased ecological and public health risks [21].

Supported catalysts have received increasing interests in heterogeneous catalysis to resolve the issue of bare NPs [22]. A variety of support materials have been investigated to immobilize/grow Pd NPs to improve the catalytic activity and selectivity in water purification applications, such as polymers, metal oxides, carbon, and silica [23-29]. In particular, mesoporous silica materials ($mSiO_2$) are widely used as catalyst supports because of their favorable features that include high surface area, controlled pore size (2-50 nm), and tunable surface charge and functional groups [30]. $mSiO_2$ supports may also be readily modified with magnetic materials (e.g., Fe_3O_4), and the obtained magnetic nano-catalysts may be efficiently isolated from reaction media through the use of an external magnet, which greatly enhances the efficiency of these catalysts and guarantees the practical industrial applications [31-33]. It should also be noted that the confined pore space of $mSiO_2$ support may control the size of the *in situ* grown Pd NPs [32, 34-36]. It has been reported that the catalytic activity of Pd-based catalysts depends on Pd NP sizes, and small

NP sizes promoted hydrogenation kinetics of various contaminants [37, 38]. Besides support pore space, the size and dispersion of *in situ* grown Pd NPs can also be influenced by the support functional group, as well as the Pd precursor [32, 39-42]. However, the influence of support functional group and Pd precursor is still insufficiently understood to obtain fine and well-dispersed Pd NPs with improved catalytic activity.

In this work, we reported the design of magnetically structured Pd-based catalysts using the synergy of magnetic materials and fine-nanoparticle Pd reactive sites. The objectives were to (1) develop and characterize Pd-based catalyst consisting of a magnetic core covered by a layer of functionalized mesoporous silica with Pd NPs grown *in situ* within the porous channels (i.e., Fe_3O_4@mSiO_2-Pd); (2) determine the influence of support functional group and Pd precursor salt on the *in situ* grown Pd NPs; and (3) evaluate the catalyst performance for the reduction of nitroarenes under mild conditions (i.e., ambient temperature and pressure) using H_2 as the reductant.

2. Experimental section

2.1 Chemicals and materials

Iron chloride ($FeCl_3$), sodium acetate (CH_3COONa), trisodium citrate ($Na_3C_6H_5O_7$), tetraethyl orthosilicate (TEOS), ammonia hydroxide solution ($NH_3 \cdot H_2O$, 28%), hexadecyltrimethyl-ammonium bromide (CTAB), (3-aminopropyl) triethocysilane (APTES), (3-mercaptopropyl) triethoxysilane (MPTES), sodium tetrachloropalladate (Na_2PdCl_4), and

palladium acetate ($Pd(OAc)_2$) were purchased from Sigma-Aldrich. Nitrobenzene ($C_6H_5NO_2$), 4-nitrophenol ($C_6H_4OHNO_2$), 2-nitrotoluene ($C_6H_4CH_3NO_2$), and 4-nitrobenzoic acid ($C_6H_4COOHNO_2$) were purchased from Alfa Aesar. Sodium dihydrogen phosphate (NaH_2PO_4), disodium hydrogen phosphate (Na_2HPO_4), isopropanol ($(CH_3)_2CHOH$), hydrochloric acid (HCl, 37%), and acetic acid (CH_3COOH) were purchased from Fisher Scientific. Ethylene glycol ($(CH_2OH)_2$), ethanol (C_2H_5OH), and methanol (CH_3OH) were purchased from BDH Chemicals. Palladium/silica powder (Pd/SiO_2, ~5% loading) from Strem Chemicals was used as a commercial Pd-based catalyst. Ultra-high purity $H_{2(g)}$ and $N_{2(g)}$ were purchased from Airgas. Ultrapure water (resistivity > 18.2 MΩ·cm) was used for all the experiments.

2.2 Catalyst preparation

2.2.1 Synthesis of magnetic (Fe_3O_4) microspheres

Magnetic Fe_3O_4 microspheres were synthesized using a hydrothermal method based on the modification of a previously reported protocol [43]. Briefly, 2.6-g $FeCl_3$, 1.5-g trisodium citrate, and 4.8-g sodium acetate were dissolved in 80 mL of ethylene glycol with magnetic stirring. The obtained yellow solution was then transferred and sealed into a Teflon-lined stainless-steel autoclave (150-mL in capacity). The autoclave was heated at 200 °C for 10 h, and then cooled to room temperature. The black products were collected and washed with ethanol and water 3 times, respectively.

To protect the magnetic Fe_3O_4 microspheres from the reaction media, a thin layer of nonporous silica was coated onto the Fe_3O_4 microspheres through a solution sol-gel method.

Briefly, aqueous Fe_3O_4 suspension was added to a three-neck round-bottom flask containing 300-mL ethanol and 5.5-mL 28% $NH_3 \cdot H_2O$ under mechanical stirring for 15 min at 30 °C (pH ~9). Afterward, 3.0-mL TEOS was added dropwise, and the reaction was allowed to proceed for 8 h under continuous mechanical stirring. The resultant product (i.e., silica coated Fe_3O_4 nanosphere) was separated and collected with a magnet, followed by washing with ethanol 6 times.

2.2.2 Growth of mesoporous silica shell and surface modification

A mesoporous silica layer was grown on the surface of silica-coated Fe_3O_4 microspheres via a controllable soft-templating approach with CTAB as the pore-directing template [17]. In a typical synthesis, 10 mL of silica-coated Fe_3O_4 suspension (~1 g) was added to a mixture containing 150-mL ethanol, 100-mL water, 1.5-g CTAB, and 2-mL 28% $NH_3 \cdot H_2O$ solution via sonication in a water bath. After mixing for 30 min, 2 mL of TEOS was added to the solution dropwise under rapid mechanical stirring, and the products were collected by a magnet after reacting at room temperature for 18 h. To remove CTAB, the solids were redispersed in a mixture containing 200-mL ethanol and 3-mL 37% HCl solution and heated under sonication at 60 °C for 2 h. This step was repeated 6 times for complete removal of CTAB. Finally, the resulting Fe_3O_4@$mSiO_2$ microspheres were collected using a magnet, washed with ethanol and water 3 times, respectively, and preserved for further modification.

The surface of Fe_3O_4@$mSiO_2$ microspheres was modified with amino (-NH_2) or thiol (-SH) groups. Briefly, 10 mL of microsphere suspension (~1 g Fe_3O_4@$mSiO_2$) was added to 90-mL isopropanol in a 250-mL two-neck bottom-round glass flask via sonication in a water bath. Then,

131 a solution containing 1.5-mL APTES or MPTES and 8-mL isopropanol was added to the reactor
132 dropwise under mechanical stirring. The solution was bubbled with $N_{2(g)}$ for 30 min to remove
133 oxygen, and then the reactor was placed in an oil bath and heated at 75 °C for 6 h under $N_{2(g)}$
134 protection. After washing with ethanol 3 times and collecting by magnetic force, the resulting
135 Fe_3O_4@mSiO_2-NH_2 (or Fe_3O_4@mSiO_2-SH) microspheres were dispersed in 40-mL water for
136 future use.

137 2.2.3 Growth of Pd NPs within Fe_3O_4@mSiO_2

138 Pd NPs were grown within the porous channels of Fe_3O_4@mSiO_2 through *in situ* reduction
139 of Pd(II) by $H_{2(g)}$ under ambient temperature and pressure [44]. Briefly, the Fe_3O_4@mSiO_2-NH_2
140 (or Fe_3O_4@mSiO_2-SH) suspension (~0.3 g of microsphere) was first diluted by 100-mL water
141 under sonication for 10 min. Subsequently, 3 mL of a Pd precursor solution (5 g/L Na_2PdCl_4 or
142 $Pd(OAc)_2$ as Pd) was added under mechanical stirring. After mixing at room temperature for 24 h,
143 the products (Fe_3O_4@mSiO_2-Pd(II)) were collected by a magnet and washed with water 3 times.
144 To obtain Fe_3O_4@mSiO_2-Pd, the as-prepared Fe_3O_4@mSiO_2-Pd(II) was dispersed in 100-mL
145 water via sonication for 10 min and then $H_{2(g)}$ was introduced to reduce the loaded Pd(II) to Pd(0)
146 at room temperature and ambient pressure under mechanical stirring for 24 h. Finally, the resultant
147 product (Fe_3O_4@mSiO_2-Pd) was collected via magnetic force, dried in a vacuum oven at 60 °C
148 for 24 h, and preserved for experimental use.

149 **2.3 Catalytic reduction experiment**

150 Catalytic reduction of representative nitroarenes (i.e., nitrobenzene, 4-nitrophenol, 2-

nitrotoluene, and 4-nitrobenzoic acid) was carried out in completely stirring batch reactors at room temperature (20 ± 2 °C) and ambient pressure (1 atm). In a typical experiment, the synthesized catalyst Fe_3O_4@mSiO_2-Pd or commercial catalyst Pd/SiO_2 was added to a 250-mL round-bottom flask with a desired solid loading to yield a concentration of 0.25 mg_{Pd}/L. The solution pH was adjusted to 7 by HCl or NaOH and maintained with a phosphate buffer. The reactor was then capped with a rubber stopper containing two 16-gauge stainless steel needles, with one serving as the $H_{2(g)}$ (1 atm) inlet and the other as both the gas outlet and the liquid sampling port. After sparging the catalyst suspension with $H_{2(g)}$ for 4 h, the reaction was initiated by injecting a desired nitroarene to yield the initial concentration of 50 mg/L, unless otherwise specified. Samples were then collected periodically, immediately filtered (0.22 μm) to quench reactions, and analyzed for nitroarene and corresponding product concentrations. To test the reusability of Fe_3O_4@mSiO_2-Pd, 50-mg/L nitrobenzene was spiked into the reactor containing Fe_3O_4@mSiO_2-Pd suspension in the interval of 30 minutes for 5 times.

2.4 Analytical methods

2.4.1 Catalyst characterization

The shape and morphology of the synthesized Fe_3O_4@mSiO_2-Pd were determined by transmission electron microscopy (TEM) and scanning electron microscopy (SEM) using a Hitachi Model H9000NAR and Hitachi Model S4800, respectively. $N_{2(g)}$ adsorption-desorption isotherms were performed with a Micromeritics ASAP-2020 Accelerated surface area and porosimetry system to measure the surface area and pore size distribution of the catalyst and support. Specific

surface area was calculated using the Brunauer–Emmett–Teller (BET) method, and pore volume and pore size distribution was obtained via the Barrett-Joyner-Halenda (BJH) model. The crystalline phases of the catalyst and support were determined by powder X-ray diffraction (XRD) measurement performed on a Bruker D8 Discover A25 diffractometer with copper Kα radiation. The surface chemical composition and states of Pd in Fe_3O_4@mSiO_2-Pd were analyzed by X-ray photoelectron spectroscopy (XPS) using a Perkin Elemer PHI 5440 ESCA system with an Al Kα X-ray source. The surface zeta potentials were measured with a Malvern Zetasizer ZS90. Concentrations of Pd in both the synthesized catalyst Fe_3O_4@mSiO_2-Pd and the commercial catalyst Pd/SiO_2 were quantified by inductively coupled plasma-optical emission spectrometry (ICP-OES, Perkin-Elmer, Model Optima 2100 DV) after digestion with HNO_3-HCl.

2.4.2 Aqueous analysis

Concentrations of nitroarenes (nitrobenzene, nitrophenol, nitrotoluene, and nitrobenzoic acid) and the corresponding reaction products were quantified by a Dionex Ultimate 3000 high performance liquid chromatography (HPLC) equipped with a Thermo Acclaim C18 column and a UV detector. The HPLC flow rate was 1.0 mL/min and a variable wavelength detector was used for the analysis. The HPLC mobile phase and detection wavelength were as below: (1) nitrobenzene, methanol and 3.3% acetic acid (70:30, v/v), at 262 nm; (2) aminobenzene, water and acetonitrile (70:30, v/v), at 230 nm; (3) nitrophenol and aminophenol, 2% acetic acid and acetonitrile (50:50, v/v), at 317 nm and 273 nm, respectively; (4) nitrotoluene and aminotoluene, methanol and water (60:40, v/v), at 266 nm and 230 nm, respectively; (5) nitrobenzoic acid and

aminobenzoic acid, methanol and 3.3% acetic acid (40:60, v/v), at 270 nm and 230 nm, respectively.

3. Results and discussion

3.1 Synthesis and characterization of Fe_3O_4@mSiO_2-Pd.

Core-shell structured magnetic catalysts Fe_3O_4@mSiO_2-Pd were prepared in five steps (Figure 1): (1) magnetic Fe_3O_4 microspheres were synthesized by hydrothermal method and the size of the spherical Fe_3O_4 core was about 200 nm (Figure 2a) [45]; (2) a thin layer of nonporous silica was coated on Fe_3O_4 nanospheres using the Stöber method to protect the magnetic core from reaction with and leaching to aqueous solutions (Figure 2b) [46]; (3) growth of mesoporous silica shell was achieved via a surfactant-templating approach using CTAB as a surfactant to control the pore size (Figure 2c) [17]; (4) the mesoporous silica layer was modified with amino group (-NH_2) using APTES or with thiol group (-SH) using MPTES after CTAB removal; and (5) the Pd source was added to the suspension of modified mesoporous support and reduced to Pd(0) NPs under room temperature and pressure using $H_{2(g)}$ (Figure 2d) [44]. Four types of synthesized catalysts (Fe_3O_4@mSiO_2-Pd) were obtained with varied combinations of modified functional groups (-NH_2 and -SH) and Pd sources (Na_2PdCl_4 and $Pd(OAc)_2$).

3.1.1 Comparison of Fe_3O_4@mSiO_2-Pd prepared from different support functional groups and Pd sources

Both the functional group of mSiO_2 support and the Pd source strongly affected the formation

and dispersion of Pd NPs within the catalyst supports. As shown in Figure 3a, the magnetic support Fe_3O_4@$mSiO_2$ was successfully developed with core-shell structure. Meanwhile, Pd NPs with quite different sizes and dispersions were observed using supports with different functional groups and Pd sources. Based on the TEM images, the use of amino-modified $mSiO_2$ support and Na_2PdCl_4 as the Pd source resulted in the uniform dispersion of Pd NPs within the support structure, compared with the other support-Pd source combinations (Figure 3). Specifically, fine Pd NPs with sizes <3 nm were formed within the amino-functionalized $mSiO_2$ shell using Na_2PdCl_4 as the Pd source (Figure 3c). The TEM-EDX spectrum of the synthesized catalyst also confirmed the existence of Pd NPs within the catalyst structure (**Figure S1** of the Supplementary Material). In contrast, Pd NPs with larger sizes and/or aggregated into larger clusters were observed for the amino-functionalized $mSiO_2$ shell with $Pd(OAc)_2$ as the Pd source (Figure 3d), thiol-functionalized $mSiO_2$ shell with Na_2PdCl_4 as the Pd source (Figure 3e), and thiol-functionalized $mSiO_2$ shell with $Pd(OAc)_2$ as the Pd source (Figure 3f).

Modification with amino groups altered the surface charge of the catalyst supports, which played an important role in the formation of fine Pd NPs. Specifically, the surface of Fe_3O_4@$mSiO_2$-NH_2 was positively charged under pH 3 – 9, while the unmodified (Fe_3O_4@$mSiO_2$) and thiol-modified (Fe_3O_4@$mSiO_2$-SH) supports were negatively charged (**Figure S2** of the Supplementary Material). Previous studies have reported a similar trend in various supports such as silica and coke that amino modification could enhance the positive charge while modification with thiol groups did not alter the surface charge significantly [47, 48]. The positive surface charge

of Fe_3O_4@mSiO_2-NH_2 may favor the interaction and immobilization of the $PdCl_4^{2-}$ ions through electrostatic attraction, thus promoting the *in situ* reduction of $PdCl_4^{2-}$ to form well-dispersed Pd NPs. On the contrary, the electrostatic repulsion between Fe_3O_4@mSiO_2-NH_2 and $Pd(OAc)_2$ and between Fe_3O_4@mSiO_2-SH and $PdCl_4^{2-}$ may negatively influence the immobilization and dispersion of Pd precursor salts onto the supports, resulting in the subsequent formation of larger Pd NPs and clusters. Interestingly, large Pd NP clusters were also formed and unevenly distributed within the negatively charged Fe_3O_4@mSiO_2-SH using $Pd(OAc)_2$ (Pd^{2+} cation) as the Pd source (Figure 3f), indicating that factors other than charge could also have a strong impact on the formation and dispersion of Pd NPs. It has been suggested that Na_2PdCl_4 could be considered an ideal Pd source for the formation of well-dispersed Pd NPs due to its solubility and the innocuous byproducts (i.e., NaCl) after reaction, among various Pd salts and Pd complexes such as $PdCl_2$, Na_2PdCl_4, $Pd(NO_3)_2$, $[Pd(NH_3)_4]Cl_2$, $[Pd(NH_3)_4](NO_3)_2$, $Pd(OAc)_2$, *tris*(dibenzylideneacetone)dipalladium $Pd_2(dba)_3$, and polynuclear hydroxo complexes (PHCs) of Pd [44, 49].

In addition, the Pd loadings of the four catalysts were determined by ICP-OES analysis after digestion with HNO_3-HCl. Highest Pd loading (4.42 wt%) was observed for the catalyst prepared with Fe_3O_4@mSiO_2-NH_2 and Na_2PdCl_4. The Pd loadings were 3.96 wt%, 2.65%, and 2.22wt% for catalysts synthesized from Fe_3O_4@mSiO_2-SH and $Pd(OAc)_2$, Fe_3O_4@mSiO_2-SH and Na_2PdCl_4, and Fe_3O_4@mSiO_2-NH_2 and $Pd(OAc)_2$, respectively. Based on the TEM images and digestion results, the catalyst prepared from Fe_3O_4@mSiO_2-NH_2 and Na_2PdCl_4 showed both a high Pd

loading and well-dispersed fine Pd NPs, and thus was selected as model catalyst for further characterization and activity evaluation in the following sections.

3.1.2 Characterization of the catalyst prepared from Fe_3O_4@mSiO_2-NH_2 and Na_2PdCl_4

A series of tools were applied to further investigate the structural and compositional properties of the catalyst prepared from Fe_3O_4@mSiO_2-NH_2 and Na_2PdCl_4 (denoted as Fe_3O_4@mSiO_2-Pd in the subsequent text for simplicity). The crystalline structure of Fe_3O_4@mSiO_2-Pd was determined by powder XRD and compared with the Pd-free supports. As shown in Figure 4a, the six characteristic peaks ($2\theta = 30.2°$, 35.6°, 43.3°, 53.8°, 57.3°, and 63.0°) in the XRD patterns matched well with the (220), (311), (400), (422), (511), and (440) reflections of Fe_3O_4 with face-centered cubic structure [50]. Additionally, a broad peak occurred at $2\theta = 24.2°$ in the XRD patterns of Fe_3O_4@mSiO_2 and Fe_3O_4@mSiO_2-Pd, but not Fe_3O_4, which may be attributed to the presence of amorphous silica in the mesoporous silica shell [51]. Meanwhile, the characteristic peaks of (111), (200), and (220) reflections of face-centered cubic metallic Pd at $2\theta = 40.2°$, 46.5°, and 67.9° were very weak and not clearly seen in the XRD pattern of Fe_3O_4@mSiO_2-Pd, which may be due to the relatively low content of Pd within the catalyst (i.e., <5 wt%) or suggest the amorphous nature of the Pd NPs grown within the mesoporous silica channel [17].

The pore structure of Fe_3O_4@mSiO_2-Pd as well as the catalyst supports was determined based on the small-angle XRD patterns (Figure 4b). The strong peak at $2\theta = 2.2°$ in the XRD patterns of Fe_3O_4@mSiO_2 and Fe_3O_4@mSiO_2-NH_2 indicated the presence of ordered hexagonal mesoporous structure and the negligible influence of amino modification on the mesoporous structure [52]. The

intensity of the characteristic peak decreased in the pattern of Fe_3O_4@mSiO_2-Pd, suggesting that the mesoporous channel became less ordered after *in situ* growth of Pd NPs. Based on the $N_{2(g)}$ adsorption-desorption isotherms (**Figure S3** of the Supplementary Material), the BET surface area and pore size of Fe_3O_4@mSiO_2-Pd were measured as 256 m^2/g and 3.0 nm, respectively. Although the growth of Pd NPs influenced the pore size and surface area of the support (**Table S1** of the Supplementary Material), our results suggested that the mesoporous structure of the catalyst was retained after *in situ* formation of Pd NPs.

The chemical composition and Pd oxidation state of Fe_3O_4@mSiO_2-Pd was investigated using XPS. The presence of Si, Pd, N, and O in the XPS survey spectrum confirmed the amino modification of Fe_3O_4@mSiO_2 and the Pd immobilization in the catalysts (Figure 5a). Based on the high-resolution Pd 3d spectrum (Figure 5b), only one set of Pd 3d spin-orbit coupling doublets was observed with the $3d_{5/2}$ binding energy at ~335 eV, indicating that no Pd species other than Pd(0) were formed during *in situ* reduction by $H_{2(g)}$ [53]. Similarly, an earlier study also reported that Na_2PdCl_4 could be readily reduced to Pd(0) NPs within carbon support in $H_{2(g)}$ at room temperature and ambient pressure [44]. Compared to conventional methods that use strong reductants and/or high temperature, the result suggested that the use of $H_{2(g)}$ at ambient temperature and pressure may be a benign and sustainable approach for the reduction of Pd(II) salts to prepare heterogeneous Pd-based catalytic materials.

3.2 Catalytic reduction of nitroarenes

4-Nitrophenol reduction was first examined at pH 7 as a model reaction to evaluate and

compare the performance between the as-synthesized catalyst Fe_3O_4@mSiO_2-Pd and a commercial catalyst Pd/SiO_2. As shown in Figure 6a, the concentration of 4-nitrophenol decreased much faster with Fe_3O_4@mSiO_2-Pd than with Pd/SiO_2, suggesting that the reaction proceeded with faster kinetics using Fe_3O_4@mSiO_2-Pd. We fitted the 4-nitrophenol reduction kinetics with the classic pseudo-first-order model (Equation 1), which has been frequently used to describe the catalytic reduction of various pollutants [54-56]:

$$\ln \frac{C_t}{C_0} = -k_{obs}t \quad (\mathbf{1})$$

where C_0 (mg/L) and C_t (mg/L) are the concentrations of 4-nitrophenol initially and at time t (h), respectively, and k_{obs} (h^{-1}) is the observed pseudo-first-order reaction rate constant. The reaction rate constant k was then calculated by normalizing k_{obs} with the mass concentration of Pd (g_{Pd}/L) into the reactor. Notably, the calculated rate constant for Fe_3O_4@mSiO_2-Pd (13,680 L/h·g_{Pd}) was ~7 times higher than that for Pd/SiO_2 (1,920 L/h·g_{Pd}), suggesting the superior reduction kinetics using Fe_3O_4@mSiO_2-Pd.

Additionally, the production of 4-aminophenol was also monitored along with 4-nitrophenol reduction to determine the overall mass balance. As shown in Figure 6b, the sum of 4-nitrophenol and 4-aminophenol concentrations were quite close to the initial concentration of 4-nitrophenol, clearly suggesting that 4-nitrophenol was selectively reduced to 4-aminophenol under the experimental condition with the use of 1 atm $H_{2(g)}$ as the reducing agent. It should be mentioned that $NaBH_4$ has been conventionally applied as a reducing agent in the catalytic reduction of nitrophenols by Pd-based catalysts in previous studies [57]. However, hydrolysis of $NaBH_4$ in

311 water was pH-dependent and may produce unwanted byproducts [58]. Meanwhile, $H_{2(g)}$ has been
312 proven as a clean and effective reducing agent in the catalytic reduction of various pollutants [9,
313 16]. Our result suggested that $H_{2(g)}$ can be efficient in the catalytic reduction of 4-nitrophenol by
314 Pd-based materials.

315 The reactivity of Fe_3O_4@mSiO_2-Pd was then investigated for the catalytic reduction of
316 several representative nitroarenes that included nitrobenzene, 2-nitrotoluene, and 4-nitrobenzoic
317 acid under neutral condition (Figure 7). Based on the fitted pseudo-first-order rate constants,
318 Fe_3O_4@mSiO_2-Pd exhibited substantially faster reaction kinetics than the commercial Pd/SiO_2 for
319 the reduction of all tested nitroarenes (Figure 7d). The improved performance of Fe_3O_4@mSiO_2-
320 Pd may be attributed to the small size and even distribution of Pd NPs within the mesoporous
321 channel. Previous study showed that the catalytic activity of conventional Pd/C was lower than
322 that of Pd/graphene oxide (Pd/GO) nanocomposites due to the smaller size and better distribution
323 of Pd NPs on GO support [59]. In the present work, the mesoporous structure and amino functional
324 groups of the Fe_3O_4@mSiO_2 support may play synergistic roles in the formation of small and well-
325 distributed Pd NPs within the support by providing abundant active sites to immobilize Pd(II)
326 precursors and confined spaces for the nucleation and growth of Pd NPs. Additionally, the
327 mesoporous structure of Fe_3O_4@mSiO_2 support may reduce the mass transfer limitation of
328 reactants and enhance the accessibility of reactive Pd sites for catalytic reduction of nitroarenes
329 [30, 60]. It was also worth mentioning that a good mass balance was achieved for the catalytic
330 reduction of all nitroarenes by Fe_3O_4@mSiO_2-Pd with $H_{2(g)}$ under ambient pressure and

temperature (**Figure S4** of the Supplementary Material), suggesting that the catalyst exhibited good selectivity for the transformation of nitroarenes to the corresponding aminoarenes.

To test the reusability of Fe_3O_4@mSiO_2-Pd, we performed a multiple spiking test by adding nitrobenzene repeatedly to the reactor every 30 minutes for 5 times. As shown in Figure 8, >98% nitrobenzene reduction was achieved even after 5 spikes, and the catalyst could be easily collected by external magnetic field. The abundant amino groups within the catalyst support may provide strong affinity to stabilize Pd NPs [61]. This feature, combined with the confined space of the mesoporous channel, may help prevent the aggregation of Pd NPs and retain the catalytic reactivity after multiple uses [17]. Further, the magnetic property of the catalyst support may facilitate catalyst recovery and reuse.

4. Conclusions

In this work, nanostructured and recyclable Pd-based catalysts were prepared based on the synergy of magnetic materials for improved catalyst recovery and fine Pd nanoparticle sites to promote catalytic reactivity. The catalyst materials consisted of a magnetic core covered by a functionalized mesoporous silica shell with Pd NPs grown within the porous channels (i.e., Fe_3O_4@mSiO_2-Pd). Fine and well-distributed Pd NPs were formed within the catalyst support modified with amino groups with the use of Na_2PdCl_4 as precursor. The Pd(II) precursor could be conveniently reduced to metallic Pd (i.e., Pd(0)) NPs through *in situ* reduction by $H_{2(g)}$ in aqueous solution under ambient temperature and pressure. The as-synthesized Fe_3O_4@mSiO_2-Pd was

efficient and outperformed commercial Pd/SiO_2 for the catalytic reduction of a suite of nitroarenes that included 4-nitrophenol, nitrobenzene, 2-nitrotoluene, and 4-nitrobenzoic acid to the corresponding aminoarenes in aqueous solution with 1 atm $H_{2(g)}$ as the reducing agent. The catalyst also showed excellent reusability and could be used to efficiently reduce nitroarenes for numerous runs. Overall, our results suggested that Fe_3O_4@mSiO_2-Pd may be an efficient and reusable catalyst for the treatment of waterborne nitroarene pollutants under ambient conditions. Furthermore, since aniline and its derivatives are important chemicals in various industries, selective reduction of nitroarene pollutants to aminoarenes may provide a potentially useful route for the production of value-added products.

Acknowledgements

This work was supported by the National Science Foundation (NSF, CBET-1932908). All opinions expressed in this work are the authors' and do not necessarily reflect the views of NSF. Y.W. acknowledges the support from Lawrence E. Sivak '71 Professorship at the University of Wisconsin – Milwaukee (UWM). We acknowledge the use of XRD, XPS, and surface analyzer at the Advanced Analysis Facility at UWM. SEM, TEM, and zeta potential measurements were performed in the Department of Biological Sciences, Department of Physics, and Water Technology Accelerator at UWM, respectively.

Figures and Captions

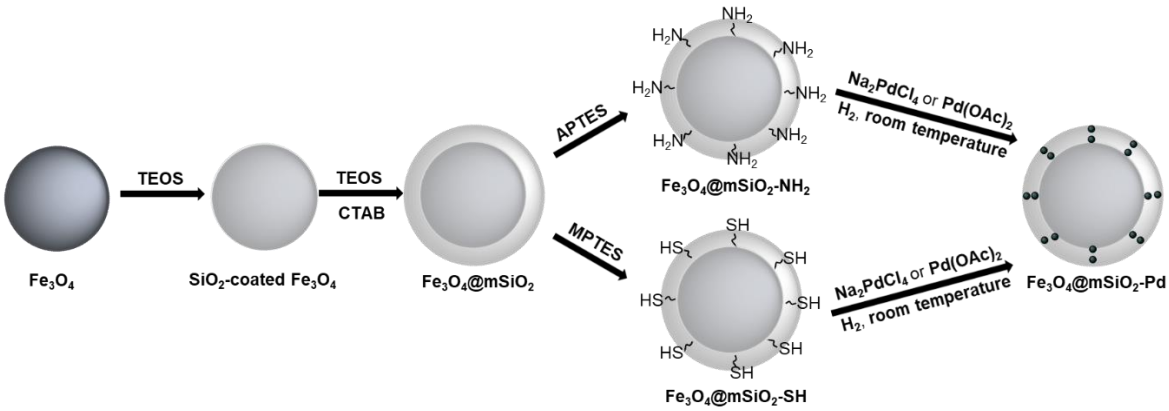

Figure 1. Schematic illustration of the preparation of Fe_3O_4@mSiO_2-Pd with various functional groups (-NH_2 or -SH) and Pd sources (Na_2PdCl_4 or $Pd(OAc)_2$).

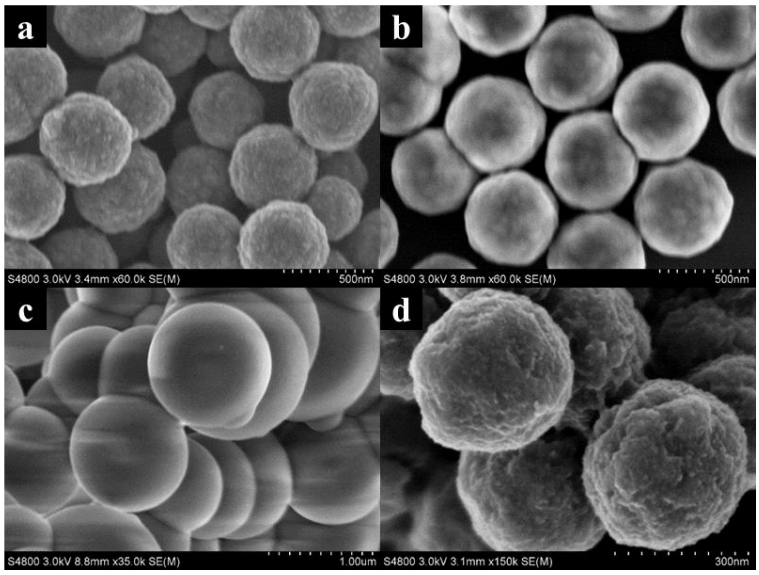

374

375 **Figure 2.** SEM images of **(a)** Fe_3O_4 microspheres, **(b)** SiO_2-coated Fe_3O_4, **(c)** Fe_3O_4@mSiO_2, and

376 **(d)** Fe_3O_4@mSiO_2-Pd.

377

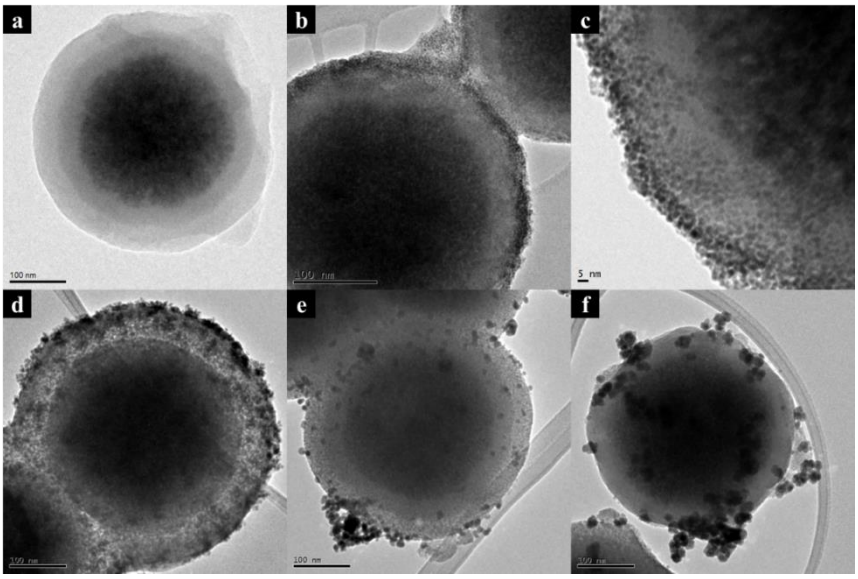

Figure 3. TEM images of **(a)** synthesized support Fe_3O_4@mSiO_2, and synthesized catalyst Fe_3O_4@mSiO_2-Pd with various functional groups and Pd sources: **(b, c)** -NH_2 and Na_2PdCl_4, **(d)** -NH_2 and $Pd(OAc)_2$, **(e)** -SH and Na_2PdCl_4, and **(f)** -SH and $Pd(OAc)_2$.

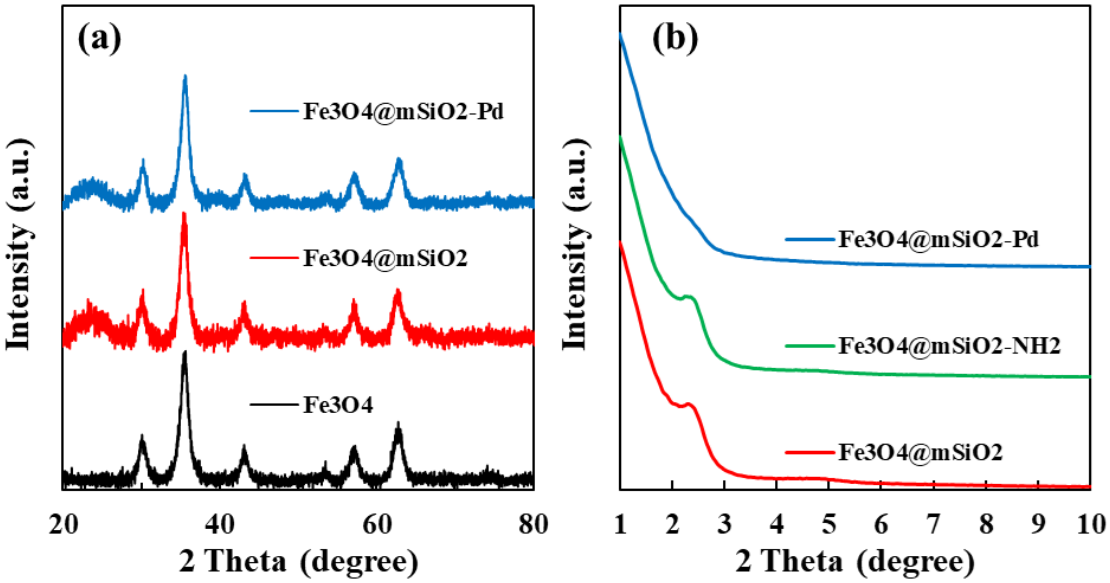

383

384 **Figure 4. (a)** Wide-angle and **(b)** small-angle XRD patterns of Fe_3O_4, Fe_3O_4@$mSiO_2$, and Fe_3O_4@

385 $mSiO_2$-Pd.

386

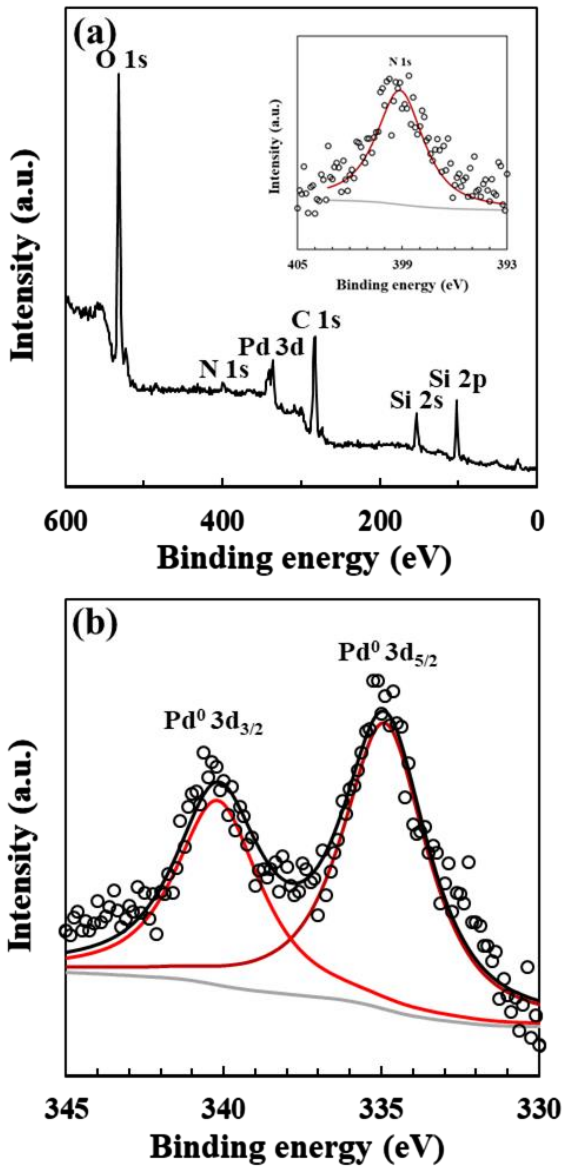

387

388 **Figure 5. (a)** XPS survey spectrum (N 1s spectrum shown in inset), and **(b)** high-resolution Pd 3d

389 spectrum of Fe_3O_4@mSiO_2-Pd.

390

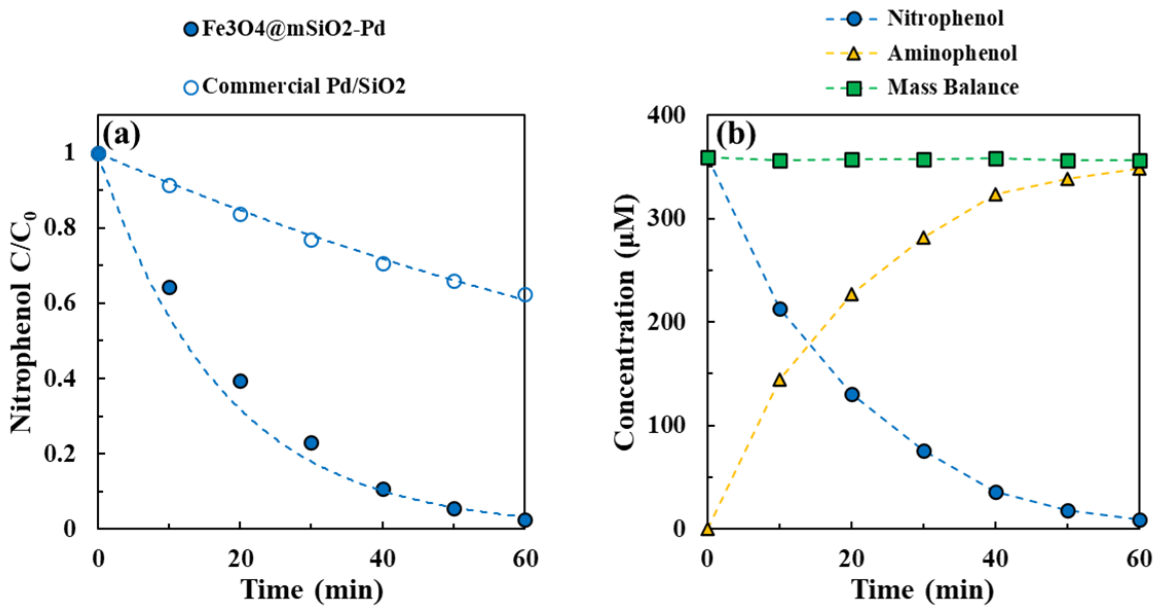

Figure 6. (a) Time courses for the reduction of 50 mg/L 4-nitrophenol by 0.25 mg_{Pd}/L loading of synthesized catalyst Fe_3O_4@mSiO_2-Pd and commercial catalyst Pd/SiO_2 in water at pH 7 and ambient temperature with 1 atm of $H_{2(g)}$. Dashed lines represent pseudo-first-order kinetics model fit. **(b)** Nitrophenol reduction and aminophenol production profiles as a function of time in the catalytic reduction of 50 mg/L 4-nitrophenol by 0.25 mg_{Pd}/L loading of synthesized catalyst Fe_3O_4@mSiO_2-Pd in water at pH 7 and ambient temperature with 1 atm of $H_{2(g)}$. "Mass balance" represents the total concentration of 4-nitrophenol and its corresponding catalytic product aminophenol.

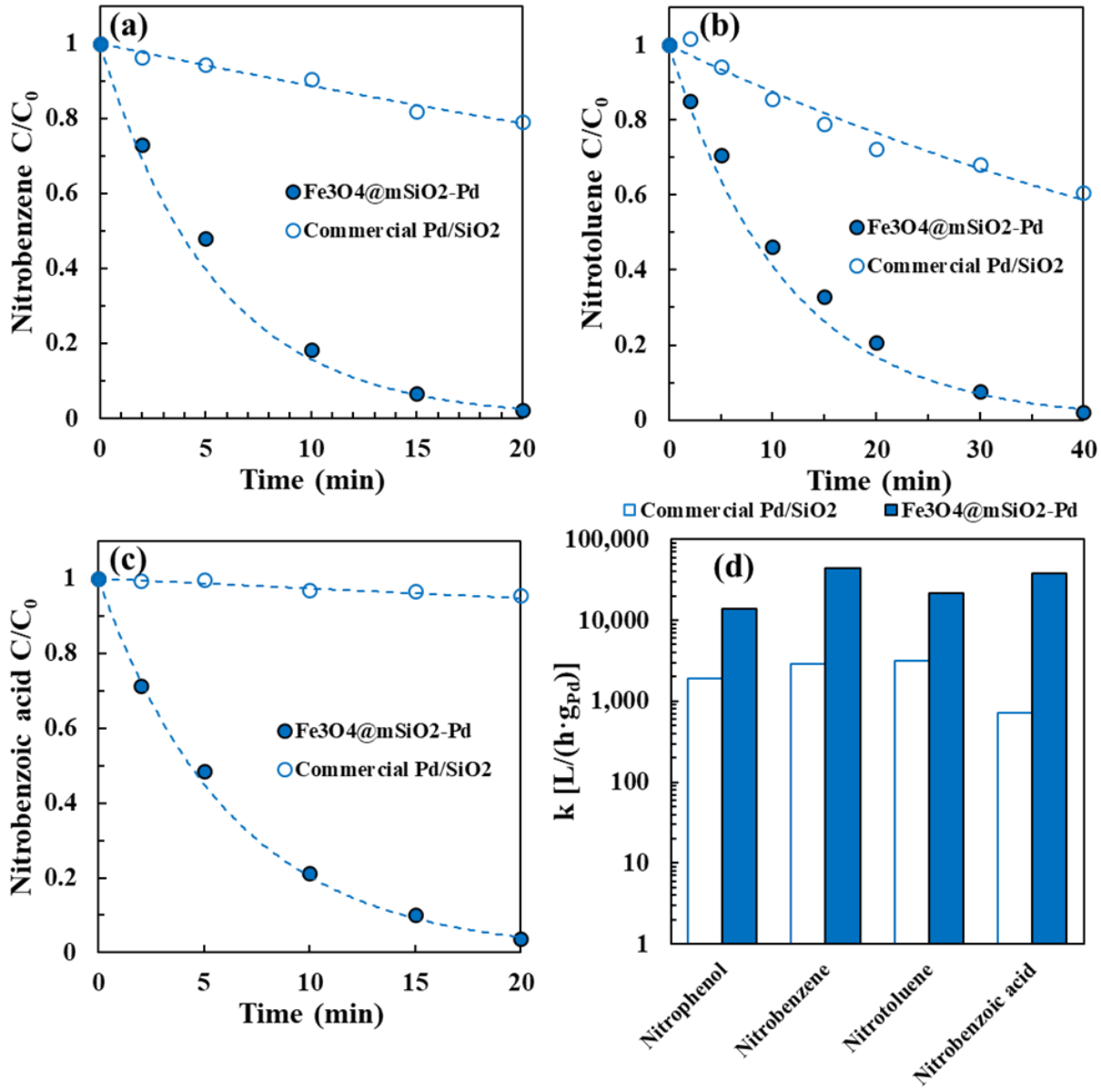

401

402 **Figure 7.** Reduction of 50 mg/L **(a)** nitrobenzene, **(b)** 2-nitrotoluene, and **(c)** 4-nitrobenzoic acid

403 by 0.25 mg_{Pd}/L loading of Fe_3O_4@mSiO_2-Pd and Pd/SiO_2 in water at pH 7 and ambient

404 temperature with 1 atm of $H_{2(g)}$. Dashed lines represent pseudo-first-order kinetics model fits.

405 Panel **(d)** shows the Pd mass-normalized rate constants for nitroarene reduction.

406

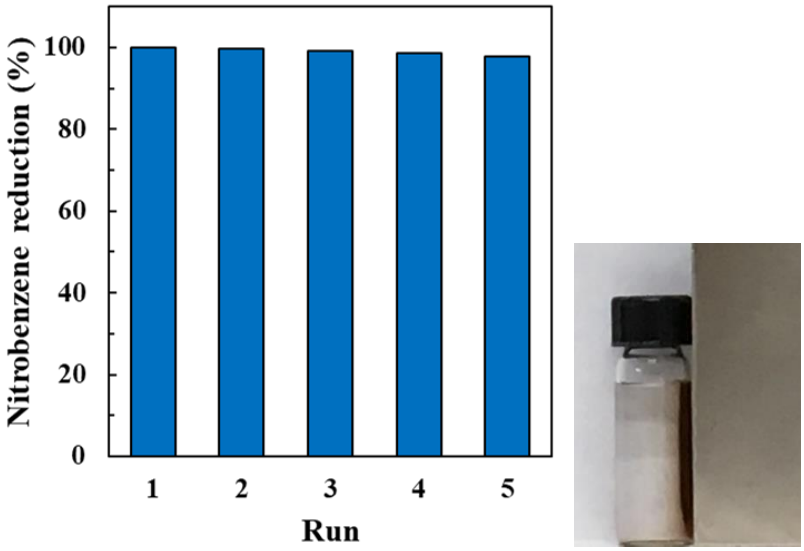

407

408 **Figure 8.** Reusability of Fe_3O_4@mSiO_2-Pd in the catalytic reduction of 50 mg/L nitrobenzene by

409 0.25 mg_{Pd}/L loading in water at pH 7 and ambient temperature with 1 atm of $H_{2(g)}$.

410

411 **References**

412 [1] M. Bilal, A.R. Bagheri, P. Bhatt, S. Chen, Environmental occurrence, toxicity concerns, and
413 remediation of recalcitrant nitroaromatic compounds, Journal of Environmental Management 291
414 (2021) 112685.
415 [2] H. Tokiwa, R. Nakagawa, K. Horikawa, A. Ohkubo, The nature of the mutagenicity and
416 carcinogenicity of nitrated, aromatic compounds in the environment, Environmental health
417 perspectives 73 (1987) 191-199.
418 [3] H. Li, Y. Cheng, H. Wang, H. Sun, Y. Liu, K. Liu, S. Peng, Inhibition of nitrobenzene-induced
419 DNA and hemoglobin adductions by dietary constituents, Applied radiation and isotopes 58(3)
420 (2003) 291-298.
421 [4] L. Carlos, D. Fabbri, A.L. Capparelli, A.B. Prevot, E. Pramauro, F.S.G. Einschlag, Intermediate
422 distributions and primary yields of phenolic products in nitrobenzene degradation by Fenton's
423 reagent, Chemosphere 72(6) (2008) 952-958.
424 [5] L. Zhao, J. Ma, Z.-z. Sun, Oxidation products and pathway of ceramic honeycomb-catalyzed
425 ozonation for the degradation of nitrobenzene in aqueous solution, Applied Catalysis B:
426 Environmental 79(3) (2008) 244-253.
427 [6] K.-S. Ju, R.E. Parales, Nitroaromatic compounds, from synthesis to biodegradation,
428 Microbiology and molecular biology reviews 74(2) (2010) 250-272.
429 [7] J. Ye, A. Singh, O.P. Ward, Biodegradation of nitroaromatics and other nitrogen-containing
430 xenobiotics, World Journal of Microbiology and Biotechnology 20 (2004) 117-135.
431 [8] M. Anjalin, N. Kanagathara, A.B. Suganthi, A brief review on aniline and its derivatives,
432 Materials Today: Proceedings 33 (2020) 4751-4755.
433 [9] N. Jadbabaei, T. Ye, D. Shuai, H. Zhang, Development of palladium-resin composites for

catalytic hydrodechlorination of 4-chlorophenol, Applied Catalysis B: Environmental 205 (2017) 576-586.

[10] S. Guo, C.D. Powell, D. Villagrán, M.S. Wong, Magnetic In–Pd catalysts for nitrate degradation, Environmental Science: Nano 7(9) (2020) 2681-2690.

[11] T. Ye, D.P. Durkin, N.A. Banek, M.J. Wagner, D. Shuai, Graphitic carbon nitride supported ultrafine Pd and Pd–Cu catalysts: enhanced reactivity, selectivity, and longevity for nitrite and nitrate hydrogenation, ACS applied materials & interfaces 9(33) (2017) 27421-27426.

[12] J.L. Cerrillo, A.E. Palomares, A review on the catalytic hydrogenation of bromate in water phase, Catalysts 11(3) (2021) 365.

[13] J. Gao, G. Chen, Q. Fu, C. Ren, C. Tan, H. Liu, Y. Wang, J. Liu, Enhancing aqueous chlorate reduction using vanadium redox cycles and pH control, Environmental Science & Technology 57(48) (2023) 20392-20399.

[14] C. Ren, E.Y. Bi, J. Gao, J. Liu, Molybdenum-catalyzed perchlorate reduction: Robustness, challenges, and solutions, ACS ES&T Engineering 2(2) (2021) 181-188.

[15] S. An, H. Ji, J. Park, Y. Choi, J.K. Choe, Influence of Chemical Structures on Reduction Rates and Defluorination of Fluoroarenes during Catalytic Reduction using a Rhodium-Based Catalyst, Chemosphere (2024) 142755.

[16] B.P. Chaplin, M. Reinhard, W.F. Schneider, C. Schüth, J.R. Shapley, T.J. Strathmann, C.J. Werth, Critical review of Pd-based catalytic treatment of priority contaminants in water, Environmental Science & Technology 46(7) (2012) 3655-3670.

[17] Y. Wang, J. Liu, P. Wang, C.J. Werth, T.J. Strathmann, Palladium Nanoparticles Encapsulated in Core–Shell Silica: A Structured Hydrogenation Catalyst with Enhanced Activity for Reduction of Oxyanion Water Pollutants, ACS Catalysis 4(10) (2014) 3551-3559.

https://doi.org/10.1021/cs500971r.

[18] J.A. Johnson, J.J. Makis, K.A. Marvin, S.E. Rodenbusch, K.J. Stevenson, Size-dependent hydrogenation of p-nitrophenol with Pd nanoparticles synthesized with poly (amido) amine dendrimer templates, The Journal of Physical Chemistry C 117(44) (2013) 22644-22651.

[19] P.K. Saikia, R.P. Bhattacharjee, P.P. Sarmah, L. Saikia, D.K. Dutta, A green synthesis of Pd nanoparticles supported on modified montmorillonite using aqueous Ocimum sanctum leaf extract: a sustainable catalyst for hydrodechlorination of 4-chlorophenol, RSC Advances 6(111) (2016) 110011-110018. https://doi.org/10.1039/C6RA22788K.

[20] V. Mazumder, S. Sun, Oleylamine-mediated synthesis of Pd nanoparticles for catalytic formic acid oxidation, Journal of the American Chemical Society 131(13) (2009) 4588-4589.

[21] K.E. Wilkinson, L. Palmberg, E. Witasp, M. Kupczyk, N. Feliu, P. Gerde, G.A. Seisenbaeva, B. Fadeel, S.-E. Dahlen, V.G. Kessler, Solution-engineered palladium nanoparticles: model for health effect studies of automotive particulate pollution, ACS nano 5(7) (2011) 5312-5324.

[22] P. Munnik, P.E. De Jongh, K.P. De Jong, Recent developments in the synthesis of supported catalysts, Chemical reviews 115(14) (2015) 6687-6718.

[23] M.M. Dell'Anna, S. Intini, G. Romanazzi, A. Rizzuti, C. Leonelli, F. Piccinni, P. Mastrorilli, Polymer supported palladium nanocrystals as efficient and recyclable catalyst for the reduction of nitroarenes to anilines under mild conditions in water, Journal of Molecular Catalysis A: Chemical 395 (2014) 307-314.

[24] P. Chen, A. Khetan, F. Yang, V. Migunov, P. Weide, S.P. Stürmer, P. Guo, K. Kähler, W. Xia, J. Mayer, Experimental and theoretical understanding of nitrogen-doping-induced strong metal–support interactions in Pd/TiO2 catalysts for nitrobenzene hydrogenation, Acs Catalysis 7(2) (2017) 1197-1206.

480 [25] Y. Wang, J. Tao, Y. Wang, L. Huang, X. Ding, Remarkable reduction ability towards p-
481 nitrophenol by a synergistic effect against the aggregation and leaching of palladium nanoparticles
482 in dendritic supported catalysts, Applied Surface Science 574 (2022) 151702.
483 [26] S. El-Hout, S. El-Sheikh, H.M. Hassan, F.A. Harraz, I. Ibrahim, E. El-Sharkawy, A green
484 chemical route for synthesis of graphene supported palladium nanoparticles: A highly active and
485 recyclable catalyst for reduction of nitrobenzene, Applied Catalysis A: General 503 (2015) 176-
486 185.
487 [27] E. Arenas-Sánchez, C.E. Niño González, V. Resendiz-Bujaidar, E. Smolentseva, B. Acosta,
488 Reduction of Nitroarenes Using Efficient PdRu@ mSiO2 Nanocatalyst Synthesized by a One-Pot
489 Approach, Advanced Materials Interfaces 11(18) (2024) 2400055.
490 [28] W. Liu, Y. Zhu, J. Wang, H. Feng, Y. Zhai, W. Li, D. Zhao, Pd/N-doped carbon dots@ dendritic
491 mesoporous silica nanospheres: A highly efficient catalyst for the hydrogenation of 4-nitrophenol,
492 Nano Research (2024) 1-8.
493 [29] V.G. Yadav, V.L. Chavan, An efficient and sustainable Pd-nanomagnetic heterogeneous
494 catalyst for the reduction of nitroarene and environmental pollutant, Applied Organometallic
495 Chemistry 37(9) (2023) e7189.
496 [30] C. Gérardin, J. Reboul, M. Bonne, B. Lebeau, Ecodesign of ordered mesoporous silica
497 materials, Chemical Society Reviews 42(9) (2013) 4217-4255.
498 [31] S. Zhao, C. Zhao, X. Li, F. Li, L. Jiao, W. Gao, R. Li, Pd nanoparticles supported on amino-
499 functionalized magnetic mesoporous silica nanotubes: a highly selective catalyst for the catalytic
500 hydrodechlorination reaction, RSC advances 6(80) (2016) 76582-76589.
501 [32] W. Li, B. Zhang, X. Li, H. Zhang, Q. Zhang, Preparation and characterization of novel
502 immobilized Fe3O4@ SiO2@ mSiO2–Pd (0) catalyst with large pore-size mesoporous for Suzuki

503 coupling reaction, Applied Catalysis A: General 459 (2013) 65-72.
504 [33] Z. Zhu, W. Wang, L. Zeng, F. Zhang, J. Liu, Selenium-directed synthesis of Pd nanoparticles
505 on mesoporous silica-coated Fe3O4: An efficient magnetic catalyst for oxidative alkene cracking,
506 Catalysis Communications 142 (2020) 106031.
507 [34] J. Ying, C. Janiak, Y.X. Xiao, H. Wei, X.Y. Yang, B.L. Su, Shape-Controlled Surface-Coating
508 to Pd@ Mesoporous Silica Core–Shell Nanocatalysts with High Catalytic Activity and Stability,
509 Chemistry–An Asian Journal 13(1) (2018) 31-34.
510 [35] I. Yuranov, P. Moeckli, E. Suvorova, P. Buffat, L. Kiwi-Minsker, A. Renken, Pd/SiO2 catalysts:
511 synthesis of Pd nanoparticles with the controlled size in mesoporous silicas, Journal of Molecular
512 Catalysis A: Chemical 192(1-2) (2003) 239-251.
513 [36] D. Shen, L. Chen, J. Yang, R. Zhang, Y. Wei, X. Li, W. Li, Z. Sun, H. Zhu, A.M. Abdullah,
514 Ultradispersed palladium nanoparticles in three-dimensional dendritic mesoporous silica
515 nanospheres: toward active and stable heterogeneous catalysts, ACS applied materials & interfaces
516 7(31) (2015) 17450-17459.
517 [37] D. Shuai, J.K. Choe, J.R. Shapley, C.J. Werth, Enhanced activity and selectivity of carbon
518 nanofiber supported Pd catalysts for nitrite reduction, Environmental science & technology 46(5)
519 (2012) 2847-2855.
520 [38] D. Shuai, D.C. McCalman, J.K. Choe, J.R. Shapley, W.F. Schneider, C.J. Werth, Structure
521 sensitivity study of waterborne contaminant hydrogenation using shape-and size-controlled Pd
522 nanoparticles, ACS Catalysis 3(3) (2013) 453-463.
523 [39] M. Martis, K. Mori, K. Fujiwara, W.-S. Ahn, H. Yamashita, Amine-functionalized MIL-125
524 with imbedded palladium nanoparticles as an efficient catalyst for dehydrogenation of formic acid
525 at ambient temperature, The Journal of Physical Chemistry C 117(44) (2013) 22805-22810.

526 [40] Y. Ding, W. Sun, W. Yang, Q. Li, Formic acid as the in-situ hydrogen source for catalytic
527 reduction of nitrate in water by PdAg alloy nanoparticles supported on amine-functionalized SiO2,
528 Applied Catalysis B: Environmental 203 (2017) 372-380.
529 [41] J. Liu, J. Hao, C. Hu, B. He, J. Xi, J. Xiao, S. Wang, Z. Bai, Palladium nanoparticles anchored
530 on amine-functionalized silica nanotubes as a highly effective catalyst, The Journal of Physical
531 Chemistry C 122(5) (2018) 2696-2703.
532 [42] J. Dobrzyńska, R. Dobrowolski, R. Olchowski, E. Zięba, M. Barczak, Palladium adsorption
533 and preconcentration onto thiol-and amine-functionalized mesoporous silicas with respect to
534 analytical applications, Microporous and mesoporous materials 274 (2019) 127-137.
535 [43] Y. Deng, Y. Cai, Z. Sun, J. Liu, C. Liu, J. Wei, W. Li, C. Liu, Y. Wang, D. Zhao, Multifunctional
536 mesoporous composite microspheres with well-designed nanostructure: a highly integrated
537 catalyst system, Journal of the American Chemical Society 132(24) (2010) 8466-8473.
538 [44] J. Gao, C. Ren, X. Huo, R. Ji, X. Wen, J. Guo, J. Liu, Supported palladium catalysts: A facile
539 preparation method and implications to reductive catalysis technology for water treatment, ACS
540 ES&T Engineering 1(3) (2020) 562-570.
541 [45] Y. Deng, D. Qi, C. Deng, X. Zhang, D. Zhao, Superparamagnetic high-magnetization
542 microspheres with an Fe3O4@ SiO2 core and perpendicularly aligned mesoporous SiO2 shell for
543 removal of microcystins, Journal of the American Chemical Society 130(1) (2008) 28-29.
544 [46] W. Stöber, A. Fink, E. Bohn, Controlled growth of monodisperse silica spheres in the micron
545 size range, Journal of colloid and interface science 26(1) (1968) 62-69.
546 [47] Z. Li, L. Wu, H. Liu, H. Lan, J. Qu, Improvement of aqueous mercury adsorption on activated
547 coke by thiol-functionalization, Chemical Engineering Journal 228 (2013) 925-934.
548 [48] W. Sheng, W. Wei, J. Li, X. Qi, G. Zuo, Q. Chen, X. Pan, W. Dong, Amine-functionalized

549 magnetic mesoporous silica nanoparticles for DNA separation, Applied Surface Science 387 (2016)
550 1116-1124.
551 [49] R.M. Mironenko, O.B. Belskaya, V.A. Likholobov, Approaches to the synthesis of Pd/C
552 catalysts with controllable activity and selectivity in hydrogenation reactions, Catalysis Today 357
553 (2020) 152-165.
554 [50] S. Xing, D. Zhao, W. Yang, Z. Ma, Y. Wu, Y. Gao, W. Chen, J. Han, Fabrication of magnetic
555 core–shell nanocomposites with superior performance for water treatment, Journal of Materials
556 Chemistry A 1(5) (2013) 1694-1700.
557 [51] V. Bansal, A. Ahmad, M. Sastry, Fungus-mediated biotransformation of amorphous silica in
558 rice husk to nanocrystalline silica, Journal of the American Chemical Society 128(43) (2006)
559 14059-14066.
560 [52] X. Min, D. Trujillo, J. Huo, Q. Dong, Y. Wang, Amine-bridged periodic mesoporous
561 organosilica nanomaterial for efficient removal of selenate, Chemical Engineering Journal 396
562 (2020) 125278. https://doi.org/https://doi.org/10.1016/j.cej.2020.125278.
563 [53] J. Liu, J.K. Choe, Z. Sasnow, C.J. Werth, T.J. Strathmann, Application of a Re–Pd bimetallic
564 catalyst for treatment of perchlorate in waste ion-exchange regenerant brine, Water Research 47(1)
565 (2013) 91-101.
566 [54] X. Min, Y. Wang, Palladium-based nanostructured catalysts for treatment of recalcitrant and
567 problematic waterborne pollutants, The World Scientific Reference of Water Science: Volume 2
568 Nanotechnology for Water Treatment and Water Interfaces, World Scientific2023, pp. 195-219.
569 [55] J. Liu, J. Gao, Catalytic reduction of water pollutants: Knowledge gaps, lessons learned, and
570 new opportunities, Frontiers of Environmental Science & Engineering 17(2) (2023) 26.
571 [56] C. Ren, P. Yang, J. Gao, X. Huo, X. Min, E.Y. Bi, Y. Liu, Y. Wang, M. Zhu, J. Liu, Catalytic

reduction of aqueous chlorate with MoO x immobilized on Pd/C, ACS Catalysis 10(15) (2020) 8201-8211.

[57] T. Aditya, A. Pal, T. Pal, Nitroarene reduction: a trusted model reaction to test nanoparticle catalysts, Chemical Communications 51(46) (2015) 9410-9431.

[58] R. Grzeschik, D. Schäfer, T. Holtum, S. Küpper, A. Hoffmann, S. Schlücker, On the overlooked critical role of the pH value on the kinetics of the 4-nitrophenol NaBH4-reduction catalyzed by noble-metal nanoparticles (Pt, Pd, and Au), The Journal of Physical Chemistry C 124(5) (2020) 2939-2944.

[59] W. Sun, X. Lu, Y. Tong, Z. Zhang, J. Lei, G. Nie, C. Wang, Fabrication of highly dispersed palladium/graphene oxide nanocomposites and their catalytic properties for efficient hydrogenation of p-nitrophenol and hydrogen generation, International journal of hydrogen energy 39(17) (2014) 9080-9086.

[60] M. Fan, W.D. Wang, Y. Zhu, X. Sun, F. Zhang, Z. Dong, Palladium clusters confined in triazinyl-functionalized COFs with enhanced catalytic activity, Applied Catalysis B: Environmental 257 (2019) 117942.

[61] H.G. Soğukömeroğulları, Y. Karataş, M. Celebi, M. Gülcan, M. Sönmez, M. Zahmakiran, Palladium nanoparticles decorated on amine functionalized graphene nanosheets as excellent nanocatalyst for the hydrogenation of nitrophenols to aminophenol counterparts, Journal of hazardous materials 369 (2019) 96-107.